JOURNAL OF NATURAL PRODUCTS

Article

pubs.acs.org/jnp

Absolute Configurations of Fungal and Plant Metabolites by Chiroptical Methods. ORD, ECD, and VCD Studies on Phyllostin, Scytolide, and Oxysporone

Giuseppe Mazzeo,[†,§] Ernesto Santoro,[†] Anna Andolfi,[‡] Alessio Cimmino,[‡] Pavle Troselj,[§,⊥] Ana G. Petrovic,[§,∥] Stefano Superchi,*[,†] Antonio Evidente,*[,‡] and Nina Berova*[,§]

[†]Dipartimento di Scienze, Università della Basilicata, Via dell'Ateneo Lucano, 10, 85100, Potenza, Italy

[‡]Dipartimento di Scienze Chimiche, Università di Napoli Federico II, Complesso Universitario Monte Sant'Angelo, Via Cintia 4, 80126, Napoli, Italy

[§]Department of Chemistry, Columbia University, 3000 Broadway, 3114, New York, New York 10027, United States

[⊥]Department of Organic Chemistry and Biochemistry, Ruder Boskovic Institute, Bijenicka c. 54, 10000, Zagreb, Croatia

[∥]Department of Life Sciences, New York Institute of Technology (NYIT), 1855 Broadway, New York, New York 10023, United States

Supporting Information

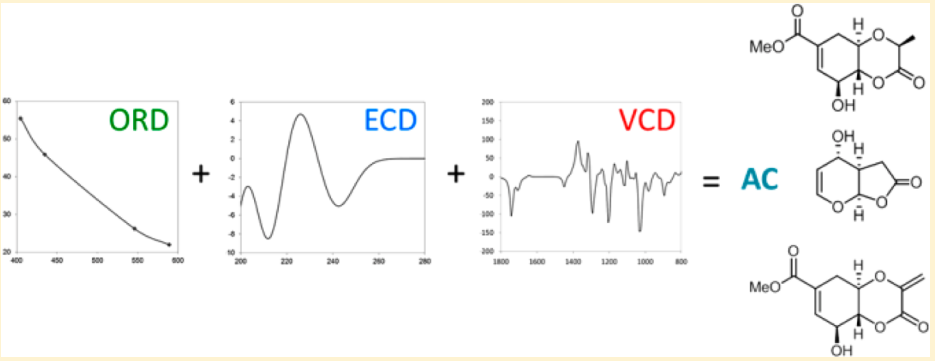

ABSTRACT: The absolute configuration (AC) of the bioactive metabolites phyllostin (**1**) and scytolide (**2**), two hexahydro-1,4-benzodioxines produced by *Phyllosticta cirsii*, and oxysporone (**3**), a dihydrofuropyranone recently isolated from a strain of *Diplodia africana*, has been assigned by computational analysis of their optical rotatory dispersion (ORD), electronic circular dichroism (ECD), and vibrational circular dichroism (VCD) spectra. Computational prediction of ORD, ECD, and VCD allowed us to assign (3*S*,4a*R*,8*S*,8a*R*) AC to naturally occurring (−)-**1**, while (4a*R*,8*S*,8a*R*) AC was assigned to (−)-**2** employing only ECD and VCD, because in this case ORD analysis turned out to be unsuitable for AC assignment. Theoretical prediction of both ORD and ECD spectra of **3** led to assignment of (4*S*,5*R*,6*R*) AC to (+)-**3**. In this case a satisfactory agreement between experimental and calculated VCD spectra was obtained only after taking into account solvent effects. This study shows that in the case of flexible and complex natural products only a concerted application of more than a single chiroptical technique permits unambiguous assignment of absolute configuration.

The assignment of absolute configuration (AC) is one of the most important and challenging tasks in the structural characterization of natural products. In fact, very often natural products are rather complex molecules, displaying many different functional groups and stereogenic centers, and endowed with high molecular flexibility. Moreover, these compounds are commonly available in small amounts from natural sources and usually do not bear heavy atoms, features that often prevent direct assignment of AC by X-ray analysis. For these reasons chiroptical methods have found broad application for configurational assignments in solution and sometimes on a microscale.[1] In addition, an increased applicability of chiroptical methods in structural analysis has been notably reinforced by the recent advances in the development of *ab initio* predictions of chiroptical properties.[2]

Although independent application of each of the three most frequently used chiroptical methods, namely, optical rotatory dispersion (ORD), electronic circular dichroism (ECD), and vibrational circular dichroism (VCD), has proved to be practical and reliable, in some cases, especially when the molecule displays high conformational flexibility, some uncertainties in the assignment are unavoidable. Therefore, for flexible molecules like some natural products, the concerted

Received: November 2, 2012
Published: February 21, 2013

application of more than one chiroptical method has recently emerged as a viable approach.[3,4]

In this paper we show that a reliable configurational assignment of complex natural products necessitates application of experimental and theoretical analysis by more than one chiroptical method. Specifically, the AC of three bicyclic fungal phytotoxins has been studied by a combined analysis of ORD, ECD, and VCD properties.

Phyllostin (**1**), scytolide (**2**), and oxysporone (**3**) (Figure 1) are of interest as promising natural herbicides for weed

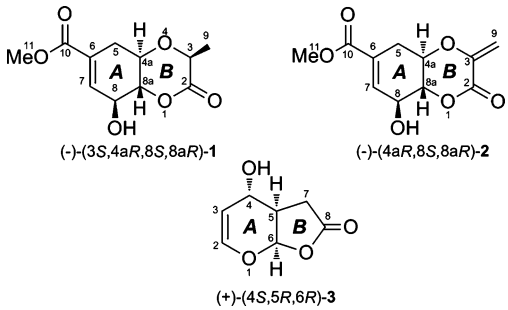

Figure 1. Structures and assigned AC of phyllostin (**1**), scytolide (**2**), and oxysporone (**3**).

biocontrol. Compound **1** was recently isolated from *Phyllosticta cirsii* fungus together with phyllostoxin[5] and phyllostictines A–D.[6] Earlier, its relative configuration was established as (3*R**,4a*S**,8*R**,8a*S**) by NMR[5] and X-ray analyses,[7] while its AC remained unknown. Total synthesis[8] and the ECD exciton chirality method[9] permitted determination of the AC of its C-8 epimer. From a more recent production of the same fungal culture filtrates, the closely related metabolite **2** was isolated and identified. Previously, **2** was obtained from *Scytalidium uredinicola*.[10] Like for **1**, the relative configuration of **2** was determined as (4a*R**,8*S**,8a*R**) by ^{1}H NMR and X-ray analyses,[10] while its AC was undefined. Also analogously to **1**, the AC of its naturally occurring C-8 epimer was determined by total synthesis.[11] Both **1** and **2** have shown promising specific activity in suicidal germination, an alternative strategy for weed control[12] of some *Orobanche* species,[13] which are parasitic weeds of important agrarian crops including tomato, cabbage, sunflower, and legumes.[14]

Compound **3** is a dihydrofuropyranone isolated for the first time from *Fusarium oxysporum*[15] and later as the main phytotoxin produced by *Pestalotia longiseta*[16] and *Pestalotiopsis oenotherae*.[17] Recently **3**, afritoxinones A and B, sphaeropsidin A, *epi*-sphaeropsidone, (*R*)-mellein, and (3*R*,4*R*)- and (3*R*,4*S*)-4-hydroxymellein were isolated from *Diplodia africana*, the causal agent of branch dieback on *Juniperus phoenicea* in Sardinia.[18] Only the relative configuration of **3** has been reported, as (4*R**,5*S**,6*S**) by NMR analysis.[15,18]

Herein we describe the assignment of the AC of metabolites **1**–**3** by concerted application of three chiroptical methods.

RESULTS AND DISCUSSION

Isolation of Compounds 1–3. Compound **1** was isolated as a white crystalline solid from the culture filtrates of *P. cirsii* as reported in the Experimental Section and identified by its spectroscopic properties (OR, UV, IR, ^{1}H and ^{13}C NMR, and ESIMS), which matched literature data.[5] Compound **2**, isolated for the first time from *P. cirsii*, was subjected to a more detailed ^{1}H and ^{13}C NMR spectroscopic analysis via COSY, TOCSY, HSQC, and HMBC experiments (Table S1). The results described are in good agreement with data based on the compound isolated from *S. uredinicola*,[10] with the exception of chemical shift assignments to C-8 and C-8a in the ^{13}C NMR spectrum, which are corrected in the present study. The structure assigned to **2** was also confirmed by its ESIMS spectrum, which showed the sodium cluster at *m*/*z* 263. The relative configuration previously assigned to **2**[10] was also confirmed by the significant couplings observed in its NOESY spectrum (see Table S1). Particularly significant are the correlation of H-4a and H-8 and the absence of correlation of H-4a and H-8a. Compound **3** was isolated from *Diplodia africana* as reported in detail in the Experimental Section and identified on the basis of spectroscopic (OR, IR, UV, ^{1}H and ^{13}C NMR, and ESIMS) data, which matched those reported.[18]

Absolute Configuration of Compounds 1–3. *Absolute Configuration of Phyllostin (1).* Taking into account the known (3*R**,4a*S**,8*R**,8a*S**) relative configuration of **1**, conformational analysis at the molecular mechanics (MM) level was carried out only on the (3*S*,4a*R*,8*S*,8a*R*)-**1** enantiomer (Figure 1), providing the five most stable conformers, differing in the orientation of the ester and hydroxy groups. In all conformers the C-3 methyl group and the C-8 hydroxy group are in pseudoequatorial orientations (Figure S1). The five MM-derived conformations were fully optimized at the DFT/B3LYP/TZVP level in the gas phase, providing four stable conformers, conformer **1c** converging into conformer **1b** (Figure 2).

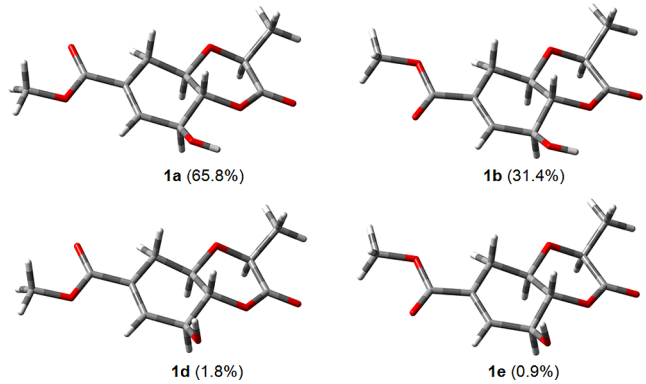

Figure 2. Most stable conformers of (3*S*,4a*R*, 8*S*, 8a*R*)-**1** calculated at the DFT/B3LYP/TZVP level of theory. Relative populations are in parentheses.

ORD and ECD Analysis. The experimental ORD curve of (−)-**1** was measured in MeOH (*c* 0.2) at four wavelengths (589, 546, 435, and 405 nm), obtaining a plane negative ORD curve increasing in absolute value at shorter wavelengths. The theoretical ORD curve was obtained by TDDFT/B3LYP/aug-cc-pVDZ calculations on conformers **1a** and **1b**, accounting for 97% of the overall population. For both conformers calculated ORDs show the same sign, trend, and order of magnitude (Table S2). After Boltzmann averaging the calculated ORD was compared with the experimental curve for (−)-**1** (Figure 3). The trend and sign of the experimental ORD is well reproduced by the theoretical curve, supporting assignment of the (3*S*,4a*R*,8*S*,8a*R*) AC for (−)-**1**.

The ECD spectrum of (−)-**1** recorded in MeOH (6.04×10^{-4} M) in the 200–300 nm range shows a negative Cotton effect (CE) at 250 nm ($\Delta\varepsilon = -1.0$) and a positive CE at 225

dx.doi.org/10.1021/np300770s | J. Nat. Prod. 2013, 76, 588–599

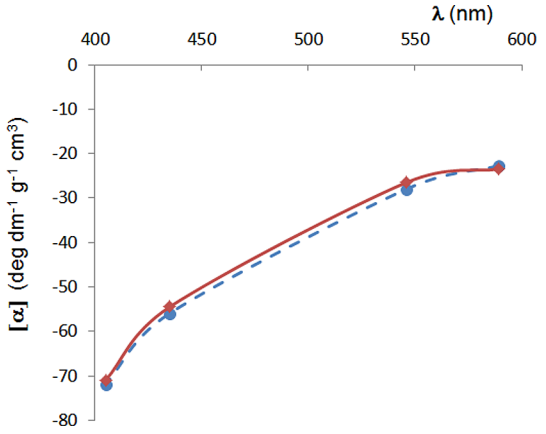

Figure 3. Calculated ORD for (3*S*,4a*R*,8*S*,8a*R*)-**1** (●, dashed blue line) and experimental ORD for (−)-**1** (♦, solid red line, *c* 0.12, MeOH).

nm ($\Delta\varepsilon$ = +3.5) followed by an emerging strong negative CE located below 200 nm (Figure 4). The ECD calculations were

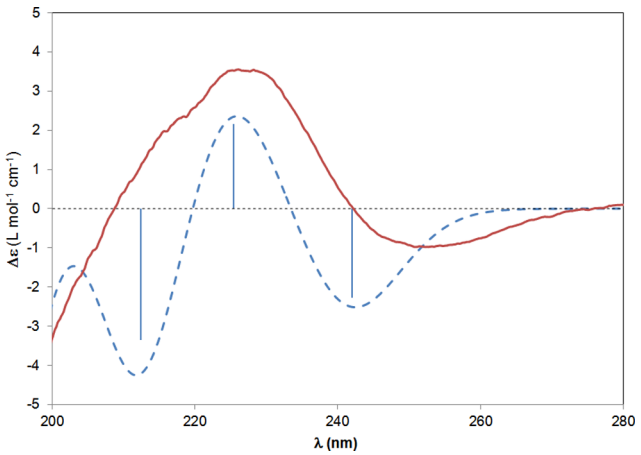

Figure 4. Experimental ECD spectrum of (−)-**1** (solid red line, MeOH) and calculated-velocity ECD spectrum of (3*S*,4a*R*,8*S*,8a*R*)-**1** (dashed blue line). Calculation of the ECD was performed at the TDDFT/CAM-B3LYP/aug-cc-pVDZ level on DFT/B3LYP/TZVP input geometries, 30 first excited states, 0.2 eV bandwidth. Vertical bars relate to rotatory strength values in velocity formalism.

performed at the TDDFT/CAM-B3LYP/aug-cc-pVDZ level of theory on the two most populated conformers, **1a** and **1b**. ECD spectra of individual conformers (Figure S2) show CEs at the same wavelength and with the same sign, implying that the relative calculated populations do not significantly affect the shape of the average ECD spectrum. The calculated ECD spectrum showed three transitions, at 210, 225, and 242 nm. As inferred from MO analysis (Figure S3) CEs at 242 and 225 nm can be ascribed to n → π^* transitions of the α,β-unsaturated ester and saturated lactone chromophores, respectively. The 210 nm band is instead assigned to the $\pi \rightarrow \pi^*$ transition of the unsaturated ester chromophore. Comparison between the calculated and experimental ECD spectra of (−)-**1** shows a satisfactory match (Figure 4). The calculated ECD spectrum reproduced the sign and intensity of the experimental CEs at 250 and 225 nm, although displaying a negative CE at 210 nm not visible in the experimental ECD spectrum. Notwithstanding these small discrepancies, this result supports assignment of (3*S*,4a*R*,8*S*,8a*R*) AC to natural compound (−)-**1**, in agreement with ORD analysis.

VCD Analysis. The vibrational absorbance (VA) and VCD spectra of (−)-**1** were recorded in DMSO-d_6 in the mid-IR region (800−2000 cm^{-1}). The vibrational activity of (−)-**1** results in 11 VA bands, six of which give rise to a VCD response (Figure 5). While bands 1−3 are more localized, the remaining eight VA bands are extensively coupled. A fairly broad spectral envelope in the region below 1500 cm^{-1} may be attributed to the presence of several closely spaced vibrational bands of the same conformer and the presence of multiple conformers of **1**. Inspection of theoretical responses of individual conformers leads to the conclusion that the latter reason is more applicable to the study of **1**, thus reconfirming the presence of four identified stable conformers. Importantly, as inferred from Figure S4, the most pronounced, diagnostic VCD bands of the most stable conformers of (−)-**1** are similar. The vibrational origin for each of the VCD bands is provided in Table 1.

In order to check whether the correlation between experimental and calculated spectra responses can be improved by accounting for the solvent effect, we applied both implicit DMSO (IEFPCM)[19] and explicit[2c] solvent models. In both cases, a redistribution of Boltzmann populations of the four conformers from the gas phase to the implicit solvation model was observed (Table S3), although with no visible changes in the geometries. The explicit solvation model, which takes into account specific intermolecular solute−solvent interactions, was obtained for each conformer found via MM search by positioning a DMSO molecule (Figure S5) so that it can interact with a hydroxy group (distance H---O: 1.73 Å). Subsequently, the intermolecular solute−solvent assemblies associated with the five conformers were submitted for optimization at the DFT/B3LYP/TZVP level of theory (Table S3).

Calculated VA and VCD spectra were computed at the B3LYP/TZVP level of theory in the gas phase, with the implicit (IEFPCM) DMSO solvation model, and with the explicit DMSO solvation model (Figure 5). It is evident from experimental−theoretical correlation that all but four VA bands (3, 4, 9, and 10) give rise to VCD signals that serve as diagnostic chirality markers of **1**. Calculated VA bands at each of the theory levels are in satisfactory correspondence with the experimental ones, despite the presence of band 8′, which has the same vibrational origin as bands 7 and 8 (O−H bending and C−O−C ester asymmetric stretching). VA bands 1 and 2 display different relative intensities in calculated vs experimental spectra. Yet, as far as AC assignment is concerned, the signs of calculated and experimental VCD bands 1 and 2 are in good agreement. Weak positive bands designated as 5/6 appear in both the experimental and calculated VCD, the latter exhibiting more pronounced rotational strengths. Negative bands 7 and 8 are well reproduced in both sign and relative intensities in experimental−calculated comparison, thus increasing the confidence level of the assignment of (3*S*,4a*R*,8*S*,8a*R*) AC to (−)-**1**.

By inspecting the VA and VCD data in Figure 5, it is evident that the best match is between the experimental curve (trace A) and the explicit model (trace B). The analogy, for example, is evident from unsplit VA band 8 in traces A and B as well as the lack of a negative VCD band at higher frequency of band 5/6 in traces A and B, but not in C and D.

dx.doi.org/10.1021/np300770s | *J. Nat. Prod.* 2013, 76, 588−599

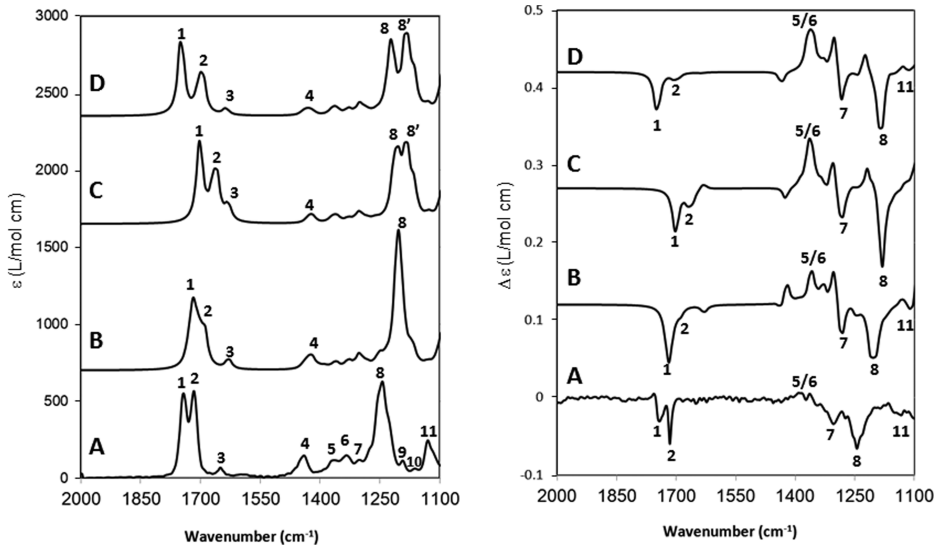

Figure 5. Experimental and calculated VA (left) and VCD (right) spectra for (−)-**1** and (3*S*,4a*R*,8*S*,8a*R*)-**1**. Trace A: Experimental in DMSO-d_6; B: DFT/B3LYP/TZVP with explicit solvent model interacting with a single DMSO molecule; C: DFT/B3LYP/TZVP implicit solvent model (IEFPCM, DMSO); D: DFT/B3LYP/TZVP, gas-phase model.

Table 1. Vibrational Origin of Normal Modes and ζ-Factor Values for VCD Bands of 1 with the Highest Rotational Strength[a]

band number	theoretical frequency (cm^{-1})	experimental frequency (cm^{-1})	vibrational origin	ζ-factor (rotatory/dipole strength)
1	1786	1744	C═O stretching of lactone within B ring	7.27 ppm
2	1758	1718	C═O stretching within ester moiety	2.62 ppm
5, 6	1415, 1389	1373, 1339	C−H bending modes of A and B rings	**39.8, 61.8 ppm**
7	1337	1320	O−H bending and C−O−C lactone asymmetric stretching	**91.5 ppm**
8	1258	1246	O−H, C−H bendings, C−O lactone stretching, and C−C−O ester asymmetric stretching	9.18 ppm
11	1150	1132	C−O stretching within the B ring coupled to C−H bending modes	**26.8 ppm**

[a]All ζ-factor values above 10 ppm are given in bold. Analysis is based on the most stable conformer associated with the explicit solvent model at the DFT/B3LYP/TZVP level of theory.

In the VCD analysis, not only of compound **1**, but also of **2** and **3**, we have recognized a need for quantitative assessment of the reliability of calculated bands, which is critical for their correlation with the experimental data. In the past few years, several VCD studies have emphasized the importance of establishing an intrinsic measure for identification of overly sensitive and, hence, unreliable calculated VCD bands. Even though the robustness concept[20] and ζ-factor analysis[21] have been applied in the analysis of a few chiral systems,[22] their suitability for broader application remains to be verified.

Herein, we recognized two situations that could potentially bring challenges for application of these methods. One is the flexible nature of the compounds, and the other is the presence of multiple transitions beneath a given VCD band. Specifically, it was found that the flexible nature of **1**−**3**, exhibited by A- and B-ring puckering modes and various dispositions of the peripheral functional groups, led to a pool of conformers with similar Boltzmann populations. In such a case, it is expected that the overall experimental spectrum will differ in the most pronounced VCD features from the individual conformers' calculated spectra. This renders assignment of one-to-one band correspondence among the theoretical traces for each conformer cumbersome, and difficult to collectively diagnose bands as reliable or not. Additionally, compounds **1**−**3** displayed multiple transitions beneath some VCD bands, thus making assessment of the overall band ambiguous. Taking into account the challenges presented by **1**−**3**, we have chosen to apply ζ-factor analysis. It should be noted that ζ-factor analysis is practical for application as the values of rotational (R) and dipole (D) strengths are listed intrinsically within an output of quantum mechanical VCD calculation. Nonetheless, the difficulty encountered in robust analysis regarding the meticulous band-to-band correspondence of calculated bands for all stable conformers with experimental bands is also present in ζ-factor analysis. As recommended,[21] ζ-factor analysis has been applied to calculated bands with significant rotational strengths of the most stable conformer.

The ζ-factor is given by the ratio of rotational and dipole strengths (R/D) and is related to the g-factor ($4R/D$).[23] When the ζ-factor is below 10 ppm, the associated band should be disregarded from the correlation.[21] As evidenced from Table 1, three out of six VCD bands have quantitatively satisfactory ζ-factor values. Bands 1 and 2 are the only ones with a localized vibrational origin, not involving stereogenic centers. It is worth mentioning that bands labeled as 5/6, 7, and 11, with satisfactory ζ-factor values, involve vibrational motion of each of the four stereogenic centers. Therefore, these bands provide a higher quantitative level of confidence for the VCD-based AC assignment of (−)-**1** as (3*S*,4a*R*,8*S*,8a*R*)-**1**. This result corroborates the AC assignment made independently via ORD and ECD analyses.

*Absolute Configuration of Scytolide (**2**).* The configurational assignment of **2** was also carried on taking into account the known (4a*R**,8*S**,8a*R**) relative configuration. The MM

dx.doi.org/10.1021/np300770s | *J. Nat. Prod.* 2013, 76, 588−599

conformational analysis on the (4a*R*,8*S*,8a*R*)-**2** enantiomer provided five stable conformers differing in the orientation of the ester and hydroxy groups (Figure S6). In all conformers the C-8 hydroxy group occupies a pseudoequatorial orientation. Full geometry optimization at the DFT/B3LYP/TZVP level in the gas phase provided four stable conformers as conformer **2c** (Figure S6) converged into conformer **2b** (Figure 6).

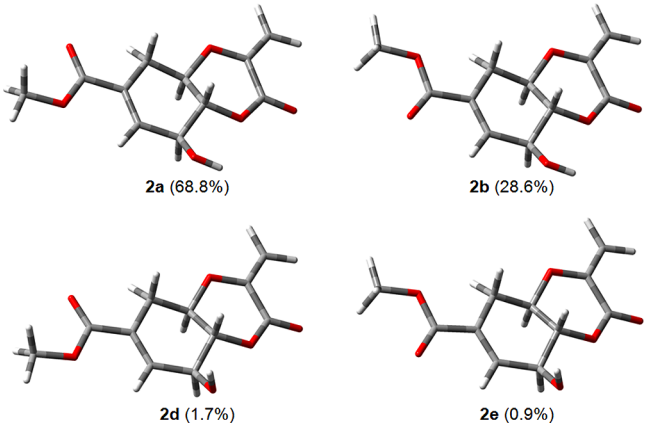

Figure 6. Most stable conformers of (4a*R*,8*S*,8a*R*)-**2** calculated at the DFT/B3LYP/TZVP level of theory. Relative populations are in parentheses.

ORD and ECD Analysis. For (−)-**2** $[\alpha]_D$ experimental values of −63.2 and −32.2 were measured in MeOH and $CHCl_3$, respectively, while $[\alpha]_D$ = −37.7 (*c* 0.26, MeOH) was reported earlier.[10] The ORD spectrum of (−)-**2** measured in MeOH and $CHCl_3$ (*c* 0.12) showed negative OR values increasing in absolute values at lower wavelengths (Figure 7). The ORD calculation was then performed at the TDDFT/B3LYP/aug-cc-pVDZ level on DFT/B3LYP/TZVP geometries of conformers **2a** and **2b**, accounting for 97% of the overall population. A

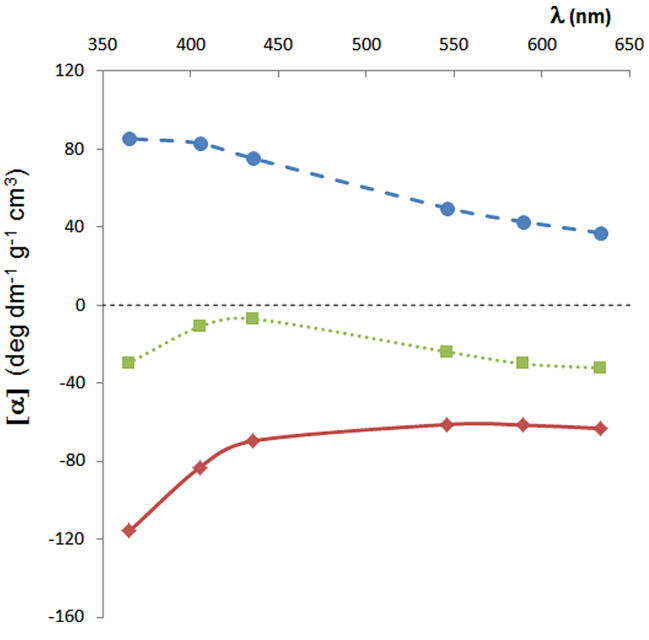

Figure 7. Calculated ORD for (4a*R*,8*S*,8a*R*)-**2** (●, dashed blue line) and experimental ORD for (−)-**2** (MeOH, ♦, solid red line and $CHCl_3$, ■, dotted green line).

calculated $[\alpha]_D$ value of +43, opposite in sign to the experimental ones, suggests that (4a*R*,8*S*,8a*R*)-**2** AC used for calculations represents the enantiomer of (−)-**2**. However, comparison between the calculated and experimental ORD of **2** (Figure 7) shows that, although the two curves are opposite in sign, they are not in a mirror image relation. The observed solvent effect also has impaired the correlation between simulated and experimental ORD curves. Interestingly, calculated ORDs for conformers **2a** and **2b** possess the same sign, trend, and order of magnitude (Table S4), showing that disagreement with the experimental curve is not due to a wrong estimate of conformer distribution. Therefore, calculations involving the solvation IEFPCM model (MeOH) were performed at the TDDFT/B3LYP/aug-cc-pVDZ(IEFPCM, MeOH) level on DFT/B3LYP/TZVP(IEFPCM, MeOH) input geometries. The PCM model implemented in geometry optimization provided a new conformer distribution (Table S5), yet the Boltzmann-weighted ORD retained the positive trend obtained in the gas-phase analysis (Table S6). Also the use of different functionals and basis sets in the calculations did not lead to appreciable changes in the ORD curve profile (Table S7). For all these reasons, computational ORD analysis of compound **2** failed to provide AC assignment.

On the other hand, ECD analysis was found to be useful for the AC determination of **2**. The ECD spectrum of (−)-**2** measured in MeOH (1.4×10^{-3} M) showed two CEs, a negative one at 240 nm ($\Delta\varepsilon$ = −2.0) and a positive one at 218 nm ($\Delta\varepsilon$ = +4.0) followed by the beginning of a strong negative CE located below 200 nm (Figure 8). The TDDFT/CAM-

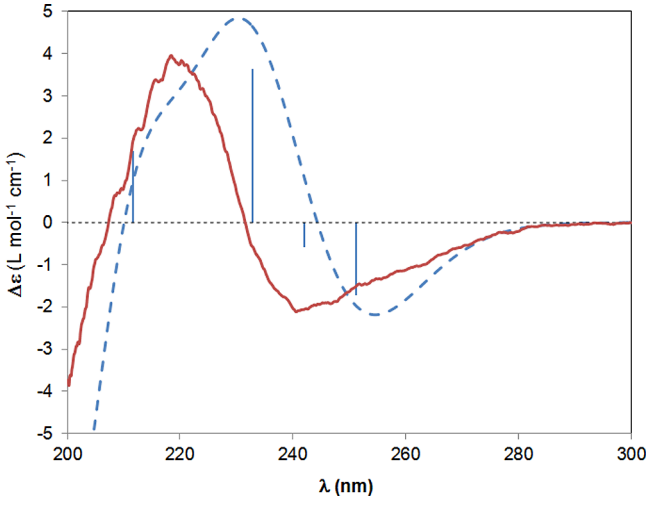

Figure 8. Experimental ECD spectrum of (−)-**2** (solid red line, MeOH) and calculated-velocity ECD spectrum of (4a*R*,8*S*,8a*R*)-**2** (dashed blue line, divided by a factor of 2). Calculation of the ECD was performed at the TDDFT/CAM-B3LYP/aug-cc-pVDZ level on DFT/B3LYP/TZVP input geometries, 30 first excited states, 0.3 eV bandwidth. Vertical bars relate to rotatory strength values in the velocity formalism.

B3LYP/aug-cc-pVDZ ECD calculations were performed for the two most populated conformers, **2a** and **2b**, as obtained by the DFT/B3LYP/TZVP level of theory for (4a*R*,8*S*,8a*R*) AC. The relative conformational distribution does not significantly affect the shape of the final Boltzmann-averaged ECD spectrum, since as shown in Figure S7, ECDs of individual conformers appear to be quite similar. The calculated ECD spectrum showed four transitions, at 250, 242, 233, and 212 nm. As inferred from MO

dx.doi.org/10.1021/np300770s | *J. Nat. Prod.* 2013, 76, 588−599

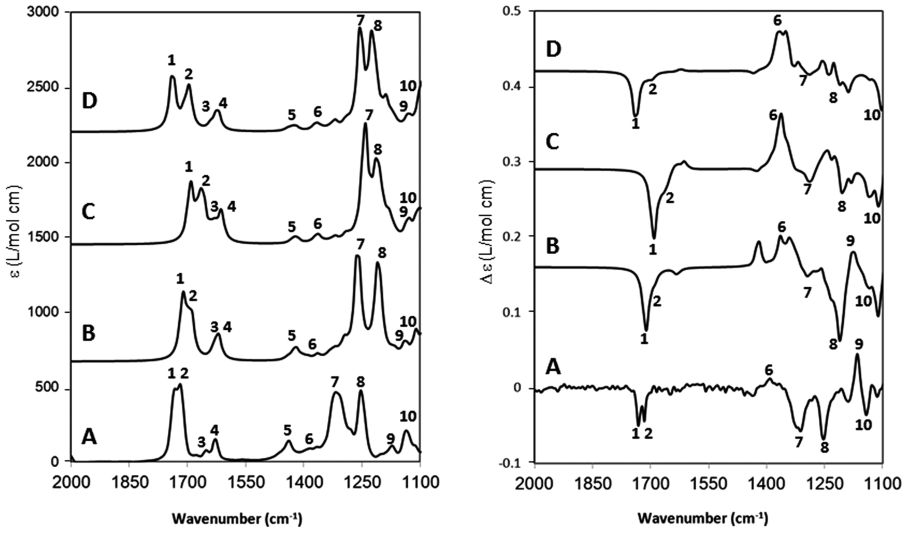

Figure 9. Experimental and calculated VA (left) and VCD (right) spectra for (−)-**2** and (4a*R*,8*S*,8a*R*)-**2**. Trace A: Experimental in DMSO-d_6; B: DFT/B3LYP/TZVP with explicit solvent model interacting with a single DMSO molecule; C: DFT/B3LYP/TZVP implicit solvent model (IEFPCM, DMSO); D: DFT/B3LYP/TZVP, gas-phase model.

analysis (Figure S8), the lower energy transitions at 250 and 242 nm, yielding a negative CE at about 260 nm, can be ascribed to n → π^* lactone and ester transitions, respectively. The 233 and 212 nm transitions are assigned to $\pi \rightarrow \pi^*$ unsaturated lactone and ester transitions, respectively. As illustrated in Figure 8, good agreement is found between the experimental and simulated ECD with respect to the sign, wavelength position, and intensity of the CEs, despite a slight red shift of the calculated curve. Clearly these ECD data alone provide unambiguous evidence for the AC assignment for natural (−)-**2** as (4a*R*,8*S*,8a*R*).

VCD Analysis. The vibrational activity of (−)-**2** results in 10 VA bands, seven of which give rise to a VCD response. Similar to **1**, while bands 1−4 are more localized, the remaining six VA bands are extensively coupled for **2** (Figure 9). The spectral envelope in the region below 1500 cm^{-1} provides additional evidence for the presence of multiple (four) stable conformers of **2** (Figure 6). The VA and VCD were reproduced at the DFT/B3LYP/TZVP level of theory in the gas phase (trace D), in implicit (IEFPCM) DMSO solvation (trace C), and in explicit DMSO (Figure S9) solvation model (trace B). The vibrational origin for the VCD bands is provided in Table 2. Figure 9 shows a comparison between experimental and calculated VA and VCD spectra computed at the three levels of theory. Regardless of the level of theory, it is evident from overall qualitative experimental−calculated correlation that seven VCD bands serve as diagnostic chirality markers of **2**. The same bands are found also present in spectra of the most stable conformers, **2a** and **2b** (Figure S10).

The overall shape of the calculated VA spectrum is in good agreement with the experimental spectrum. Calculated bands 1 and 2 are split just like the experimental bands. Calculated VA bands 3 and 4 appear as a single peak, while the experimental ones are more distinct. Furthermore, experimental band 5 is not as distinct in the calculated spectrum, while bands 7, 8, 9, and 10 are well reproduced. In the calculated VCD, bands 1 and 2 are not split as in the experimental, but they both reproduced the negative sign seen in the experimental spectrum. The remaining bands are not readily correlating at the level of theory involving gas-phase calculation (Figure 9, trace D).

Table 2. Vibrational Origin of Normal Modes and ζ-Factor Values for VCD Bands of 2 with the Highest Rotational Strength[a]

band number	theoretical frequency (cm^{-1})	experimental frequency (cm^{-1})	vibrational origin	ζ-factor (rotatory/ dipole strength)
1	1781	1744	C═O stretching of lactone within B ring	**12.9 ppm**
2	1759	1718	C═O stretching within ester moiety	2.17 ppm
6	1477	1412	O−H bending and CH_3 ester bending	**81.1 ppm**
7	1314	1318	C−O−C lactone asymmetric stretching coupled to C−H bending	4.58 ppm
8	1260	1253	C−C−O asymmetric stretching coupled to C−H bending	9.00 ppm
9	1225	1166	C−H bending (twisting) within A ring	**894 ppm**
10	1156	1132	C−O lactone stretching coupled to C−H bending modes	**18.4 ppm**

[a]All ζ-factor values above 10 ppm are given in bold. Analysis is based on the most stable conformer associated with the explicit solvent model at the DFT/B3LYP/TZVP level of theory.

Implicit solvation model calculation was performed by application of the IEFPCM DMSO model (Figure 9 C). As in the case of **1**, reoptimization at the IEFPCM level of theory redistributed the Boltzmann populations of the four conformers with respect to gas-phase calculation (Table S8), but no significant structural changes occurred in conformer geometries. In the implicit model, calculated VCD bands 7 and 8 are more negative and better defined than in the gas phase. However matching of implicit model calculation and experimental VCD traces is still unsatisfactory. Specifically problematic for correlation with experimental VCD is the presence of a positive band between VCD bands 7 and 8. Therefore, the explicit solvent model, calculated at the DFT/

B3LYP/TZVP level, has been considered (Table S8). Figure 9B shows that the explicit DMSO model provided a better correlation of both VA and VCD spectra with respect to experimental: VCD band 2 appears as a shoulder of band 1; VA band 6 is now well reproduced in intensity; VCD bands 7 and 8 are now clearly negative; and VCD bands 9 and 10 also become well correlated.

To assess the quantitative reliability of the theoretical VCD bands, calculated normal modes of (4a*R*,8*S*,8a*R*)-**2** have been subjected to ζ-factor analysis. As evidenced from Table 2, (4a*R*,8*S*,8a*R*)-**2** displays four out of seven bands as quantitatively satisfactory by ζ-factor analysis.[21] With the exception of band 1, the bands with high ζ-factor values, namely, bands 6, 8, 9, and 10, involve vibrational motion of one or more stereogenic centers of **2**. Band 8, which is related to vibrations of stereogenic carbons, also marginally approaches the borderline of ζ-factor criteria (~9 ppm).[21] Overall, we consider that four bands provide a higher quantitative level of confidence for the VCD-based AC assignment.

Overall, VCD-based analysis supports the ECD-based AC assignment of (−)-**2** as (4a*R*,8*S*,8a*R*). However, the unexpected disagreement between the simulated and experimental ORD data of **2**, a close structural analogue of **1**, prevents the AC assignment by the ORD approach. The reason for this intriguing discrepancy will be the subject of future studies.

*Absolute Configuration of Oxysporone (**3**).* Taking into account the known (4*R**,5*S**,6*S**) relative configuration of **3**, conformational analysis at the MM level was performed on the (4*R*,5*S*,6*S*)-**3** enantiomer, providing six conformers within a 10 kcal/mol energy window that differed by the orientation of the hydroxy group and the sense of twist of the five- and six-membered rings. The hydroxy group occupies both pseudoequatorial and pseudoaxial orientations. The MM-obtained conformers were fully optimized at the DFT/B3LYP/cc-pVTZ level of theory, providing six conformers, **3a**–**f**. The three most stable ones, **3d**, **3f**, and **3e**, account for 97% of the overall population (Figure 10). These conformers possess P twist of the B ring, with the hydroxy group in a pseudoaxial orientation, and differ in O−H bond orientation.

ORD and ECD Analysis. The experimental ORD spectrum of (+)-**3** (Figure 11) was measured in EtOH (*c* 0.5) and in $CHCl_3$ (*c* 0.7), showing in both solvents plane positive curves with solvent-independent $[\alpha]$ values. The ORD calculations were performed at the TDDFT/B3LYP/aug-cc-pVDZ level on DFT/B3LYP/cc-pVTZ level optimized geometries of

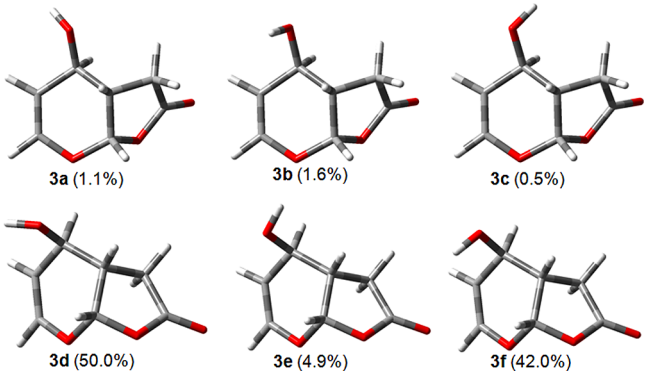

Figure 10. The most stable conformers of (4*R*,5*S*,6*S*)-**3** calculated at the DFT/B3LYP/cc-pVTZ level. Relative populations are in parentheses.

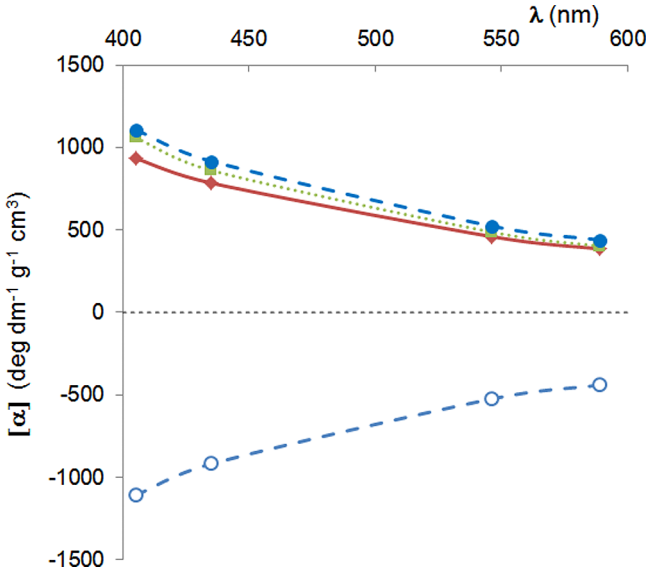

Figure 11. Calculated ORD for (4*R*,5*S*,6*S*)-**3** (○, dashed blue line) and that of opposite enantiomer (4*S*,5*R*,6*R*)-**3** (●, dashed blue line) and experimental ORD for (+)-**3** (EtOH, ♦, solid red line and $CHCl_3$, ■, dotted green line).

(4*R*,5*S*,6*S*)-**3**, leading to a calculated plane negative ORD curve as a mirror image with similar absolute $[\alpha]$ values to the experimental curve (Figure 11 and Table S9). Comparison of the experimental ORD with the calculated curve for the opposite (4*S*,5*R*,6*R*)-**3** enantiomer supports assignment of (4*S*,5*R*,6*R*) AC for **3**.

The ECD spectrum of (+)-**3** measured in MeCN (8.6×10^{-3} M) showed a low-amplitude negative CE at 230 nm ($\Delta\varepsilon$ = −0.2) and a strong positive CE at 200 nm ($\Delta\varepsilon$ = +24.0) (Figure 12). The TDDFT ECD calculation was performed at the TDDFT/CAM-B3LYP/aug-cc-pVDZ level of theory on

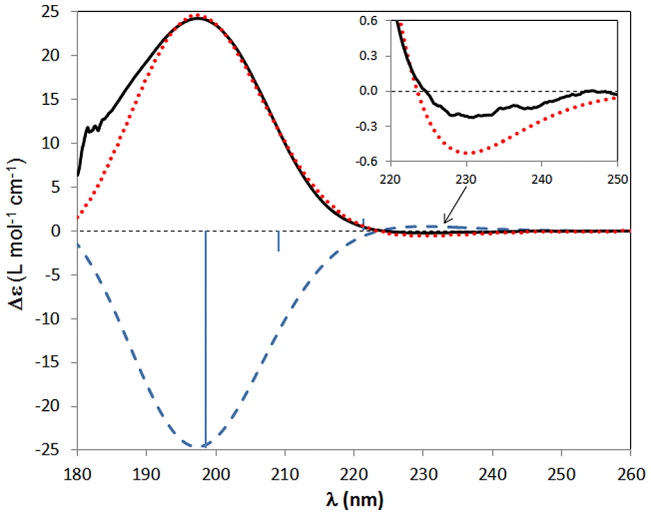

Figure 12. Experimental ECD spectrum of (+)-**3** (solid black line, MeCN) and calculated ECD spectra for (4*R*,5*S*,6*S*)-**3** (dashed blue line) and (4*S*,5*R*,6*R*)-**3** (dotted red line). Calculation of the ECD was performed at the TDDFT/CAM-B3LYP/aug-cc-pVDZ level on DFT/B3LYP/TZVP input geometries, 30 first excited states, 0.4 eV bandwidth. Vertical bars relate to rotatory strength values in the velocity formalism. Upper-right box: zoom-in of the calculated (dotted red line) and experimental (solid black line) negative 230 nm CEs.

dx.doi.org/10.1021/np300770s | *J. Nat. Prod.* 2013, 76, 588−599

DFT/B3LYP/cc-pVTZ-optimized geometries. The ECDs of single conformers are quite similar in trend and signs; therefore the relative population of conformers does not affect the shape of the final Boltzmann-averaged ECD spectrum. The calculated ECD spectrum showed three transitions, at 198, 210, and 220 nm. As inferred from MO analysis (Figure S11) the weak positive CE at 230 nm can be ascribed to the n → π^* transition of the lactone moiety, while the strong negative CE at about 200 nm originates from two negative rotatory strengths of the π → π^* transitions of the double-bond chromophores. In Figure 12 it is evident that the computed and experimental ECD spectra for (4*R*,5*S*,6*S*)-**3** and (+)-**3** reflect a near mirror image relationship, strongly supporting opposite (4*S*,5*R*,6*R*) AC for (+)-**3**.

VCD Analysis. The vibrational activity of (+)-**3** results in 11 VA bands, all of which give rise to a VCD response. Figure 13

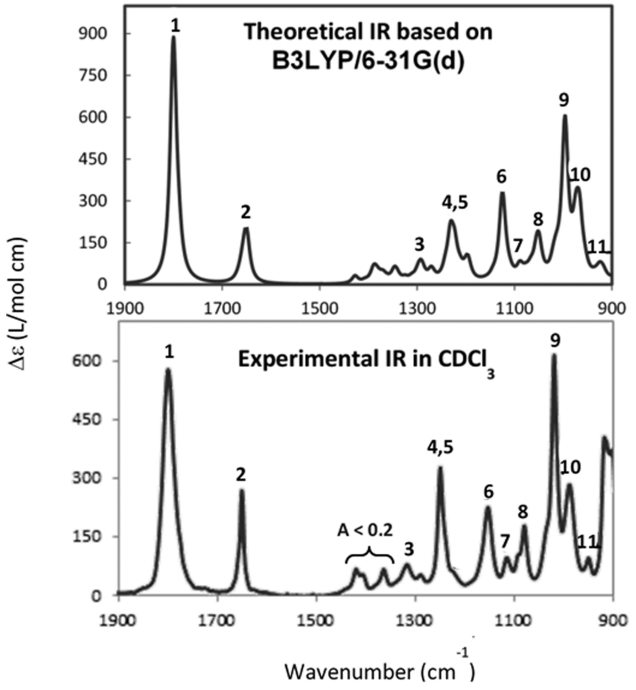

Figure 13. Comparison of VA bands between Boltzmann-weighted spectra at the B3LYP/6-31G(d) level of theory and experimental bands for **3**.

displays a satisfactory agreement in relative positions and intensity for 11 experimental and theoretical Boltzmann-weighted bands at the B3LYP/6-31G(d) level of theory. This quantitative correlation validates the presence of six stable conformers, **3a**−**f**, of (4*R*,5*S*,6*S*)-**3**.

As mentioned earlier, the more planar ring disposition is found for less stable conformers **3a**−**c**. On the other hand, in the case of conformers **3d**−**f**, ring B puckers out of plane of the A ring. The structural uniformity displayed by **3a**−**c** and **3d**−**f**, respectively, is reflected in the uniformity of the theoretically predicted VCD response (Figure S12). The dominantly populated **3d**−**f** exhibit a more pronounced VCD in the 900−1100 cm^{-1} region, manifested as more distinct VCD bands in the Boltzmann-weighted spectrum.

The experimental−calculated spectra comparison indicates that VCD bands of (+)-**3** do not match the simulated data for (4*R*,5*S*,6*S*)-**3**. In fact, the calculated VCD trace of the (4*S*,5*R*,6*R*) model closely resembles the experimental trace (Figure 14). The predicted spectra responses obtained via the B3LYP/6-31G(d) gas-phase level of theory for the three most stable conformers, **3d**−**f** (Figure S12), are similar, while the remaining three conformers display differences in VCD band distribution and signs, especially below 1400 cm^{-1}. The spectra variation can be attributed to differences in the A- and B-ring puckerings, which consequently alter the relative disposition of electric and magnetic transition dipoles originating from ring C−H bending modes.

The correspondence of the calculated VCD for the (4*S*,5*R*,6*R*) model with the experimental VCD is, however, not optimal at the B3LYP/6-31G(d) level of theory (Figure 14). While bands 1−11 exhibit qualitative correlation between experimental and theoretical spectra, three predicted VCD bands, labeled by stars, are not observed in the experimental spectrum.

To address the mismatch regions, we resorted to a higher level of theory along with a closer analysis of the experimental conditions. First, it was recognized that the weak intensity of the experimental IR bands in the ∼1300−1500 cm^{-1} region justifies the lack of distinct VCD bands that most likely arise from the baseline noise. Even though the combination of concentration and path length has been adjusted to maximize the experimental response in the entire 900−2000 cm^{-1} window, VCD bands in this challenge region remain negligible due to IR intensities below 0.2 unit.

Resorting to higher level basis sets, gas-phase B3LYP/6-311++G(2d,2p) and gas-phase B3LYP/aug-cc-pVTZ did not resolve these inconsistencies. As is evident in Figure 15, the D and E traces with unresolved bands 1 and 9 are less optimal in matching the experimental spectrum than trace C. Figure 15A−E shows that only the B3LYP/6-31G(d) theoretical implicit model accounting for the presence of $CHCl_3$ solvent provides a considerably more satisfactory correspondence. Resorting to the IEFPCM-6-31G(d) level of theory does not affect the geometries of the stable conformers and relative populations. Specifically in terms of VCD, the IEFPCM-6-31G(d) level of theory improves the correlation by eliminating the extra band present between bands 7 and 8 in the B3LYP/6-31G(d) gas-phase calculation (Figure 14), thus providing a more optimal match with the experimental spectrum (Figure 16). The origin of the vibrational bands is listed in Table 3. To test the reliability of the theoretical bands, we have applied ζ-factor[21] analysis (see Experimental Section). Table 3 shows that the ζ-factor provides a quantitative confidence for the reliability of all, except band 1. While bands 2−11 display ζ-factors greater than 10 ppm, for band 1 this parameter is less optimal, namely, 0.69 ppm.

The vibrational origin of bands indicates that only bands 1 and 2 originate from localized transitions. Specifically, band 1 is associated with pronounced C_8═O stretch, while band 2 is associated with pronounced C-2−C-3 stretch, and none of the involved carbons (C-2, C-3, and C-8) are stereogenic centers. These localized, decoupled modes are not the most optimal diagnostic markers of the AC. The remaining nine bands (bands 3−11) display satisfactory ζ-factor values (>10 ppm), which raises the confidence level of the VCD-based AC assignment. Many of these bands are combinations of several normal modes associated with one of the three stereogenic centers. Based on the overall VCD analysis, the sound correlation among 10 of the 11 VCD bands of (+)-**3** leads to the AC assignment as (4*S*,5*R*,6*R*).

dx.doi.org/10.1021/np300770s | *J. Nat. Prod.* 2013, 76, 588−599

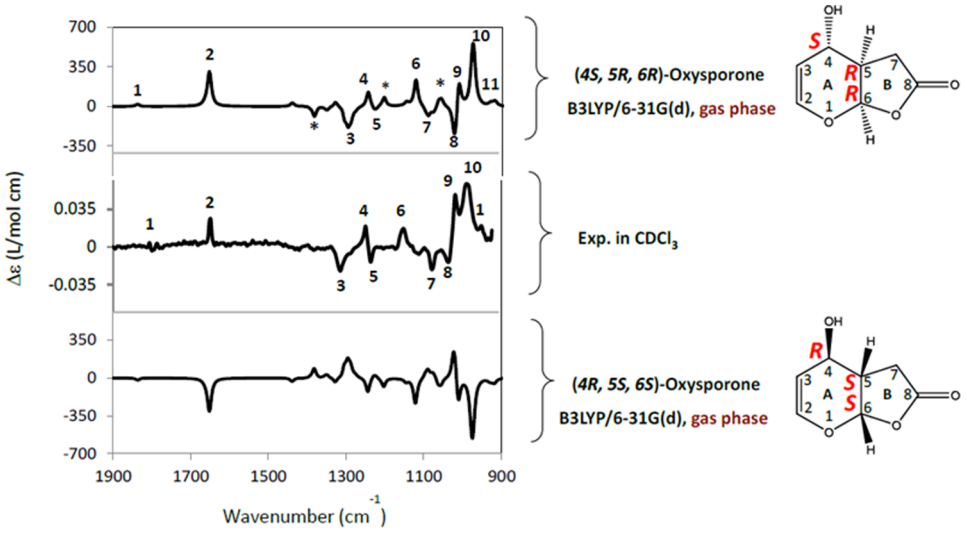

Figure 14. Correlation between experimental VCD bands of (+)-**3** and B3LYP/6-31G(d)-calculated spectra traces for (4*R*,5*S*,6*S*)-**3** and (4*S*,5*R*,6*R*)-**3**.

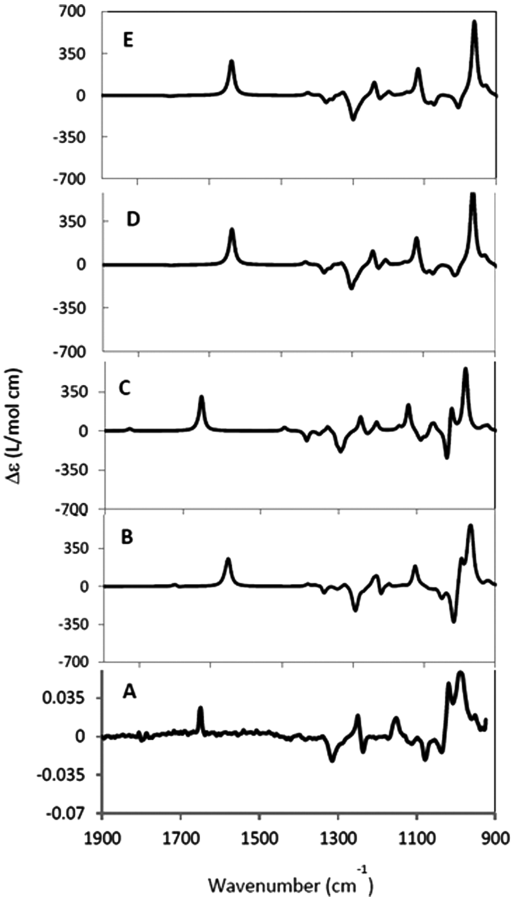

Figure 15. Correlation between experimental VCD bands of (+)-**3** and calculated spectra of (4*S*,5*R*,6*R*)-**3** at different levels of theory: (A) experimental spectrum of (+)-**3**; (B) implicit solvation IEFPCM-6-31G(d), (C) gas-phase/6-31G(d); (D) gas-phase/6-311++G(2d,2p); (E) gas-phase/aug-cc-pVTZ.

CONCLUSION

The assignment of the ACs of fungal phytotoxins **1**−**3** has been addressed by concerted use of ORD, ECD, and VCD spectroscopy. In the case of phyllostin (**1**), computational prediction of ORD fully matched experimental data, while ECD and VCD predictions, although satisfactorily reproducing experimental chiroptical properties, showed some small differences. The combined application of these three approaches permitted the reliable assignment of (3*S*,4a*R*,8*S*,8a*R*) AC to naturally occurring (−)-**1**, which is supported by the known relative configuration assignments. In scytolide (**2**), while theoretical analysis of both electronic and vibrational CD provided clearly interpretable and consistent results, ORD analysis was found unsuitable because of the discrepancy between calculated and experimental ORD curves. Therefore, in the case of (−)-**2**, only two of the applied chiroptical methods allow for a reliable AC assignment as (4a*R*,8*S*,8a*R*). The good agreement between experimental and calculated ORD and ECD spectra of oxysporone (**3**) led to unequivocal AC assignment. Taking into account the solvent effects, all of the calculated VCD bands resulted in a satisfactory agreement with the experimental spectrum. Consequently, all three chiroptical methods support the AC assignment of (+)-**3** as (4*S*,5*R*,6*R*).

In summary, this study clearly supports the idea that when dealing with structurally complex and flexible molecules, like naturally occurring phytotoxins **1**−**3**, a concerted application of more than one chiroptical methodology should be considered as a preferable approach. Often in such cases, when applied independently, these methods do not provide sufficiently reliable evidence for an unambiguous AC assignment. With respect to VCD analysis, additional assessment of quantitative reliability of theoretical bands, as by ζ-factor analysis in the current study, may enhance the diagnostic relevance with respect to determination of molecular chirality.

EXPERIMENTAL SECTION

General Experimental Procedures. Melting points were measured on an Axioskop Zeiss microscope coupled with a Mettler FP90 electric hot plate. Compounds **1**−**3** were identified by optical rotation at 589 nm, measured on Jasco P-1010 and Jasco DIP370 digital polarimeters; IR spectra were recorded as glassy film on a Perkin-Elmer Spectrum One FT-IR spectrometer, and UV spectra were taken on both a Perkin-Elmer Lambda 25 UV/vis and a JASCO V-530 spectrophotometer. ORD spectra were recorded on a Jasco DIP370 digital polarimeter, and ECD spectra were recorded on a

dx.doi.org/10.1021/np300770s | J. Nat. Prod. 2013, 76, 588−599

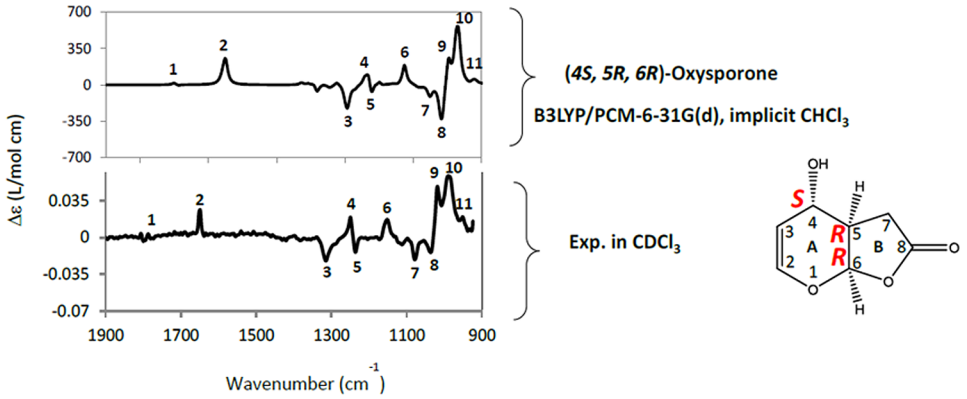

Figure 16. Band-to-band correlation between experimental VCD for (+)-**3** and IEFPCM-6-31G(d) VCD bands of (4*S*,5*R*,6*R*)-**3**.

Table 3. Vibrational Origin of IEFPCM-6-31G(d) Theoretically Predicted Bands along with ζ-Factor Values for VCD Bands of 3 with Highest Rotational Strength[a]

band number	theoretical frequency (cm^{-1})	experimental frequency (cm^{-1})	vibrational origin	ζ-factor (rotatory/dipole strength)
1	1873	1801	C═O stretching of the B ring	0.69 ppm
2	1715	1650	pronounced C═C stretching	**33.7 ppm**
3	1346	1303		**109 ppm**
4	1292	1247	C−H bending modes (wagging) coupled to C−O bending of the A ring	**48.6 ppm**
5	1272	1222		**12.6 ppm**
6	1170	1150	asymmetric C−C(carbonyl)−O stretching within the lactone of the B ring	**11.7 ppm**
7	1092	1072	C−C stretching within the A ring	**12.4 ppm**
8	1061	1029	C−C stretching within the A and B rings	**120 ppm**
9	1036	1019	C−O stretching within A and B rings coupled to C−C stretching within the A ring	**12.5 ppm**
10	1005	984	C−OH stretching coupled to breathing modes of the A ring	**47.5 ppm**
11	958	943	C−H wagging modes of the A ring	**13.3 ppm**

[a]All ζ-factor values above 10 ppm are given in bold.

JASCO J-810 spectropolarimeter. ^1H and ^{13}C NMR spectra were recorded on Bruker spectrometers at 600 and 125 MHz, respectively; ^{13}C multiplicities were determined by DEPT spectra. DEPT, COSY-45, TOCSY, HSQC, HMBC, and NOESY experiments were performed using Bruker microprograms. ESIMS spectra were recorded on an Agilent Technologies Quadrupole LC/MS 6120. Analytical and preparative TLC were performed on silica gel (Merck, Kieselgel 60 F_{254}, 0.25 and 0.50 mm) plates; the spots were visualized by exposure to UV light and/or by spraying first with 10% H_2SO_4 in MeOH and then with 5% phosphomolybdic acid in EtOH, followed by heating at 110 °C for 10 min. Column chromatography was performed on silica gel (Merck, Kieselgel 60, 0.063−0.200 mm).

VA and VCD spectra of **1**, **2**, and **3** were recorded in the mid-IR region (800−2000 cm^{-1}) on a Fourier transform Jasco FVS-6000 VCD spectrometer. Spectra measurements of **1** and **2** were made at concentrations of 0.297 and 0.290 M, respectively, in DMSO-d_6 in a fixed 50 μm path-length BaF_2 cell. A total of 12 000 scans (equivalent to 2 h data accumulation time) at 4 cm^{-1} resolution have been employed for spectra recording. Spectra measurement of **3** was done at a concentration of 0.474 M in $CDCl_3$ in a fixed-path-length cell with BaF_2 windows and a 50 μm spacer. A total of 6000 scans (equivalent to 1 h data accumulation time) at 4 cm^{-1} resolution have been employed for spectra recording.

Fungal Strain. The strain of *Phyllosticta cirsii* used to produce **1** and **2** was identified by Dr. Alexander Berestetskiy (All-Russian Institute of Plant Protection, Russian Academy of Agricultural Sciences, Pushkin, Saint-Petersburg, Russia) and deposited with number A-10 in the collection of the same institute. The strain of *Diplodia africana* used to produce **3** was identified by Dr. Benedetto Linaldeddu (Università di Sassari, Dipartimento di Agraria, Sezione Patologia Vegetale e Entomologia, Sassari, Italy) and deposited with number DA1 in the collection of the same department.

Production, Purification, and Identification of Fungal Metabolites. Compound **1** was produced growing *P. cirsii* as previously reported.[5] The fungal culture filtrates were extracted with EtOAc and purified, yielding phyllostictines A−D and **1** (0.9 mg/L) as white crystals. The organic extract (2.56 g) obtained from other culture filtrates (8.3 L) of the same fungus was purified by chromatography on a silica gel column as previously reported.[5] The residue of fraction 2 (800 mg) showed by TLC (EtOAc−*n*-hexane, 6:4 v/v) the presence of two metabolites, the minor of which was **1**. This residue was further purified by silica gel CC to afford two crystalline compounds (R_f 0.72 and 0.58), the most polar of which was identified as **1** (1.2 mg/L). Compound **1** showed mp 138−142 °C, $[\alpha]^{25}_D$ −29.4 (*c* 0.1, MeOH), and spectroscopic data (IR, UV, ^1H and ^{13}C NMR, and ESIMS) in agreement with the literature.[5] The main compound was identified as **2** (72.3 mg/L): $[\alpha]^{25}_D$ −63.2 (*c* 0.30, MeOH); UV (MeCN) λ_{max} (ε) nm 217 (11 700); IR ν_{max} 3405, 1716, 1651, 1626, 1245 cm^{-1} (lit.:[10] $[\alpha]_D$ −37.7 (*c* 0.26, CH_3OH); IR (KBr) 3430, 1725, 1709, 1654, 1627 cm^{-1}; UV (MeOH) 214 (12,100); ^1H and ^{13}C NMR see Table S1; ESIMS *m*/*z* 263 $[M + Na]^+$. Compound **3** was produced by growing *D. africana* as recently reported.[18] According to this procedure the fungal culture filtrates were acidified at pH 4, extracted with EtOAc, and purified to yield **3** as a homogeneous oil (29.7 mg/L). Isolated compound **3** showed $[\alpha]_D$ = +365 (*c* 0.5, $CHCl_3$) and spectroscopic data (IR, UV, ^1H and ^{13}C NMR, and ESIMS) in agreement with the literature.[18]

Computational Details. Preliminary conformational analysis was performed by the Spartan 02[24] package using the MMFF94s molecular mechanics force field and Monte Carlo search on chosen ACs

dx.doi.org/10.1021/np300770s | *J. Nat. Prod.* 2013, 76, 588−599

(3*S*,4a*R*,8*S*,8a*R*)-**1**, (4a*R*,8*S*,8a*R*)-**2**, and (4*R*,5*S*,6*S*)-**3**. After surveying the conformational space, the geometries within a 10 kcal/mol energy window were subjected to *ab initio* energy minimization as implemented in the Gaussian 09 package.[25] Specifically, the DFT/B3LYP/TZVP level was employed for **1** and **2**, while **3** was subjected to the DFT/B3LYP level of theory by resorting to four combinations of basis sets as well as an implicit solvation model: gas-phase/6-31G(d), gas-phase/cc-pVDZ, gas-phase/6-311++G(2d,2p), gas-phase/aug-cc-pVTZ, implicit solvation IEFPCM-6-31G(d). All conformers of **1**−**3** are real minima, as no imaginary vibrational frequencies were found. Free energies were calculated and used to determine the Boltzmann populations of the conformers at 298.15 K.

Calculations of ORD and ECD spectra were performed at the TDDFT level of theory using either the B3LYP or CAM-B3LYP functional, respectively, and the aug-cc-pVDZ basis set. The use of the long-range corrected CAM-B3LYP functional[26] provided better ECD spectra simulation results than the more common B3LYP functional.[27] The theoretical ORD, ECD, and VCD spectra were obtained as weighted averages of Boltzmann populations. The ECD spectra, in particular, were obtained from calculated excitation energies and rotational strengths as a sum of Gaussian functions centered at the wavelength of each transition with a parameter σ (width of the band at half-height) of 0.3 or 0.4 eV and elaborated using the SpecDis v1.51 program.[28] To guarantee origin independence and to evaluate the quality of the molecular wave functions employed,[29] calculated ECD spectra were obtained in both the length and velocity form, using the lowest 30 states. In all cases the velocity/length-calculated spectra were almost coincident, indicating a good level of calculation. Therefore, in all figures only the velocity-form-predicted spectra are reported. The theoretical VA and VCD spectra were simulated with Lorentzian band shapes and 10 cm^{-1} half-width at half of peak height. The frequencies of each of the theoretical spectra have been scaled by a scaling factor: B3LYP/6-31G(d) gas phase, the scaling factor was 0.9613; B3LYP/PCM-6-31G(d) implicit $CHCl_3$, the scaling factor was 0.9613; B3LYP/6-311++G(2d,2p) gas phase, the scaling factor was 0.9700; B3LYP/aug-cc-pVTZ gas phase, the scaling factor was 0.9676.[30]

To assess the reliability of the predicted signs and intensities of VCD bands, the vibrational normal modes of the most stable conformers were subjected to ζ-factor analysis.[21] To perform ζ-factor analysis, the absolute values of rotational (R) and dipole (D) strengths have been extracted from the Gaussian (G-09) output file. The ζ-factor was determined by taking the ratio between rotational and dipole strengths: for the ith band, $\zeta_i = R_i/D_i$.

■ ASSOCIATED CONTENT

Ⓢ Supporting Information

^1H and ^{13}C NMR data of scytolide (**2**), MM conformer structures, single conformer calculated ORD, ECD, and VCD spectra for **1**−**3**, calculated MOs associated with main **1**−**3** electronic transitions. This material is available free of charge via the Internet at http://pubs.acs.org.

■ AUTHOR INFORMATION

Corresponding Author

*(S.S.) Tel: +39 0971-20-2232. Fax: +39-0971-20-2223. E-mail: stefano.superchi@unibas.it. (A.E.) Tel: + 39 081-253-9178. Fax: +39-081-253-9186. E-mail: evidente@unina.it. (N.B.) Tel: +1 212-854-3934. Fax: +1-212- 932-1289. E-mail: ndb1@columbia.edu.

Notes

The authors declare no competing financial interest.

■ ACKNOWLEDGMENTS

The authors thank Dr. M. Vurro and Dr. M. C. Zonno (CNR, Istituto di Scienze delle Produzioni Alimentari, Italy), Dr. A. Berestetskiy (All-Russian Institute of Plant Protection, Russian Academy of Agricultural Sciences, Russia), and Prof. L. Maddau (Università di Sassari, Dipartimento di Agraria, Sezione di Patologia Vegetale, Italy) for the culture filtrates of *P. cirsii* and *D. africana*, respectively. Prof. K. Nakanishi (Columbia University, USA), Dr. G. A. Ellestad (Columbia University, USA), and Prof. N. Harada (Tohoku University, Japan) are gratefully acknowledged for helpful discussions as well as Mrs. D. Melck (CNR, Istituto di Chimica Biomolecolare, Italy) for recording the NMR spectra of scytolide. The authors appreciate also the instrumental and technical support of JASCO Corp., Japan, and JASCO, Inc. USA, and the financial support from the Università della Basilicata and MIUR (Rome) (PRIN Project 2008LYSESR).

■ REFERENCES

(1) Berova, N.; Ellestad, G. A.; Harada. N. In *Comprehensive Natural Products II Chemistry and Biology*; Mander, L., Lui, H.-W., Eds.; Elsevier: Oxford, 2010; Vol. *9*, Chapter 4, pp 91−146.

(2) For general discussion of the *ab initio* calculation of chiroptical properties: (a) Autschbach, J. *Chirality* **2009**, *21*, E116−E152. (b) Autschbach, J.; Nitsch-Velasquez, L.; Rudolph, M. *Top. Curr. Chem.* **2011**, *298*, 1−98. (c) Guochun, Y.; Yunjie, X. *Top. Curr. Chem.* **2011**, *298*, 189−236.

(3) (a) Polavarapu, P. *Chirality* **2008**, *20*, 664−672. (b) Stephens, P. J.; McCann, D. M.; Devlin, F. J.; Cheeseman, J. R.; Frisch, M. J. *J. Am. Chem. Soc.* **2004**, *126*, 7514−7521. (c) Polavarapu, P. L.; Donahue, E. A.; Shanmugam, G.; Scalmani, G.; Hawkins, E. K.; Rizzo, C.; Ibnusaud, I.; Thomas, G.; Habel, D.; Sebastian, D. *J. Phys. Chem. A* **2011**, *115*, 5665−5673.

(4) Superchi, S.; Rosini, C.; Mazzeo, G.; Giorgio, E. Determination of Molecular Absolute Configuration: Guidelines for Selecting a Suitable Chiroptical Approach. In *Comprehensive Chiroptical Spectroscopy: Applications in Stereochemical Analysis of Synthetic Compounds, Natural Products, and Biomolecules*; Berova, N.; Polavarapu, P. L.; Nakanishi, K.; Woody, R. W., Eds.; John Wiley & Sons, Inc.: Hoboken, NJ, USA, 2012; Vol. *2*, Chapter 12, pp 421−447.

(5) Evidente, A.; Cimmino, A.; Andolfi, A.; Vurro, M.; Zonno, M. C.; Motta, A. *J. Agric. Food Chem.* **2008**, *56*, 884−888.

(6) Evidente, A.; Cimmino, A.; Andolfi, A.; Vurro, M.; Zonno, M. C.; Cantrell, C. L.; Motta, A. *Tetrahedron* **2008**, *64*, 1612−1619.

(7) Tuzi, A.; Andolfi, A.; Cimmino, A.; Evidente, A. *J. Chem. Crystallogr.* **2010**, *40*, 15−18.

(8) Muralidharam, V. B.; Wood, H. B.; Ganem, B. *Tetrahedron Lett.* **1990**, *31*, 185−188.

(9) Isogai, A.; Washizu, M.; Murakoshi, S.; Suzuki, A. *Agric. Biol. Chem.* **1985**, *49*, 167−169.

(10) Ayer, W. A.; Fukazawa, Y.; Orszanska, H. *Nat. Prod. Lett.* **1993**, *2*, 77−82.

(11) (a) Teng, C. P.; Yukimoto, Y.; Ganem, B. *Tetrahedron Lett.* **1985**, *26*, 21−24. (b) Chouinard, P. M.; Bartelett, P. A. *J. Org. Chem.* **1986**, *51*, 75−78.

(12) Yoneyama, K.; Awad, A. A.; Xie, X.; Yoneyama, K.; Takeuchi, Y. *Cell. Physiol.* **2010**, *51*, 1095−1103.

(13) Evidente, A.; et al. Unpublished results (Prof. Diego Rubiales of the Institute for Sustainable Agriculture, CSIC, Cordoba, Spain, Personal Communication).

(14) Evidente, A.; Abouzeid, M. A.; Andolfi, A.; Cimmino, A. *J. Agric. Sci. Technol.* **2011**, *A1*, 461−483.

(15) Adegosan, E. Y.; Alo, B. I. *Phytochemistry* **1979**, *18*, 1886−1887.

(16) Nagata, T.; Ando, Y. *Agric. Biol. Chem.* **1989**, *53*, 2811.

(17) Venkatasubbaiah, P.; Van Dyke, C. G.; Chilton, W. S. *Phytochemistry* **1991**, *30*, 1471−1474.

(18) Evidente, A.; Masi, M.; Linaldeddu, B. T.; Franceschini, A.; Scanu, B.; Cimmino, A.; Andolfi, A.; Motta, A.; Maddau, L. *Phytochemistry* **2012**, *77*, 245−250.

(19) Mennucci, B.; Tomasi, J. *J. Phys. Chem. A* **2002**, *106*, 6102−6113.

(20) (a) Nicu, V. P.; Neugebauer, J.; Baerends, E. J. *J. Phys. Chem. A* **2008**, *112*, 6978−6991. (b) Nicu, V. P.; Baerends, E. J. *Phys. Chem.*

Chem. Phys. **2009**, *11*, 6107−6118. (c) Nicu, V. P.; Baerends, E. J. *Chirality* **2010**, *21*, E287−E297. (d) Nicu, V. P.; Baerends, E. J. Complexation, Solvation, and Chirality Transfer in Vibrational Circular Dichroism. In *Comprehensive Chiroptical Spectroscopy: Applications in Stereochemical Analysis of Synthetic Compounds, Natural Products, and Biomolecules*; Berova, N.; Polavarapu, P. L.; Nakanishi, K.; Woody, R. W.; Eds.; John Wiley & Sons, Inc.: Hoboken, NJ, USA, 2012; Vol. *1*, Chapter 26, pp 747−781.
(21) Gobi, S.; Magyarfalvi, G. *Phys. Chem. Chem. Phys.* **2011**, *13*, 16130−16133.
(22) Rode, J. E.; Dobrowolski, J. C. *Chirality* **2012**, *24*, 5−16.
(23) Kuhn, W. *Trans. Faraday Soc.* **1930**, *26*, 293−308.
(24) *SPARTAN 02*; Wavefunction, Inc.: Irvine, CA.
(25) Frisch, M. J.; et al. *GAUSSIAN 09*, Revision A.02; Gaussian, Inc.: Wallingford, CT, 2009.
(26) Yanai, T.; Tew, D. P.; Handy, N. C. *Chem. Phys. Lett.* **2004**, *393*, 51−57.
(27) For a recent example of use of the CAM-B3LYP functional see: Evidente, A.; Superchi, S.; Cimmino, A.; Mazzeo, G.; Mugnai, L.; Rubiales, D.; Andolfi, A.; Villegas-Fernandez, A. M. *Eur. J. Org. Chem.* **2011**, 5564−5570.
(28) Bruhn, T.; Hemberger, Y.; Schaumlöffel, A.; Bringmann, G. *SpecDis* version 1.51; University of Wuerzburg: Germany, 2011.
(29) Moscowitz, A. In *Modern Quantum Chemistry*; Sinanoglu, O., Ed.; Academic Press: London, 1965; Part III, p 31.
(30) (a) Merrick, J. P.; Moran, D.; Radom, L. J. *Phys. Chem. A* **2007**, *111*, 11683−11700. (b) Singha, P.; Boesch, S. E.; Gu, C.; Wheeler, R. A.; Wilson, A. *J . Phys. Chem. A* **2004**, *108*, 9213−9217.